Ordinary state-based peridynamics for thermoviscoelastic deformation

E. Madenci* and S. Oterkus**

* Department of Aerospace and Mechanical Engineering
University of Arizona, Tucson, United States of America

** Department of Naval Architecture, Ocean and Marine Engineering
University of Strathclyde, Glasgow, United Kingdom

This study presents the ordinary state-based peridynamic (PD) constitutive relations for viscoelastic deformation under mechanical and thermal loads. The behavior of the viscous material is modeled in terms of Prony series. The constitutive constants are the same as those of the classical history-integral model, and they are also readily available from relaxation tests. The state variables are conjugate to the PD elastic stretch measures; hence, they are consistent with the kinematic assumptions of the elastic deformation. The PD viscoelastic deformation analysis successfully captures the relaxation behavior of the material. The numerical results concern first the verification problems, and subsequently, a double-lap joint with a viscoelastic adhesive where failure nucleates and grows.

1. Introduction

Many structural materials exhibit viscoelastic behavior under high temperature applications. Polymers and solid-propellant materials are usually modeled as linear viscoelastic materials. Viscoelasticity is the property of materials that exhibit both viscous and elastic characteristics when undergoing deformation. Its response depends on loading rate, deformation history and its rate. Therefore, critical structures made of viscoelastic materials warrant the search for a better understanding of their mechanical behavior, including failure characteristics. Their time dependent behavior modeled by using Prony series is well understood from a computational point of view within the Classical Continuum Mechanics (CCM), and commercially available finite element programs enable the prediction of their response without any difficulty.

Keywords: peridynamics, viscoleasticity, isotropic, prony series, failure

However, the CCM faces conceptual and mathematical challenges when addressing crack nucleation and growth especially in the presence of multiple crack paths. These challenges stem from the fact that the equations of CCM involve spatial derivatives of the displacement components, and do not contain an internal length scale. Peridynamics (PD), a reformulation of the CCM by Silling (2000) and Silling et al. (2007) removes these challenges by introducing an internal length scale, and integro-differential equations as opposed to the partial differential equations of CCM. It is extremely suitable for failure analysis of structures because it allows cracks to nucleate and grow naturally. An extensive literature survey on PD is given by Madenci and Oterkus (2014).

The PD theory is not limited to elastic material response. Mitchell (2011) presented the ordinary state-based PD viscoelastic model, and studied the relaxation response of a single bond in the case of a two parameter PD standard linear solid model. Also, Weckner and Mohamed (2013) developed a bond-based PD micromodulus with viscoelastic effects. By considering an infinite viscoelastic bar subjected to a dynamic point load, they showed that the PD theory recovers the local viscoelastic response in the limit as the PD internal length approaches zero.

This study may be considered as an extension of Mitchell's pioneering study that employs the Strain Energy Density (SED) function suggested by Silling et al. (2007) for the " *linear PD solid* ". The main contribution concerns the use Prony series for modeling the behavior of viscous material for three- and two-dimensional PD thermoviscoelastic analyses. Also, it employs the PD form of the SED function suggested by Madenci and Oterkus (2014) for a linear material response identical to that of classical continuum mechanics. It is expressed in terms of three PD material parameters specifically for small deformation and small rotations. These PD parameters for both three- and two-dimensional analyses are determined by calibration against the classical SED by considering the two simple loading conditions of isotropic expansion and simple shear.
However, this SED function employs a specific form of the weight function suggested by Madenci and Oterkus (2014) because it recovers the bond-based PD formulation.

After performing its verification by comparison with finite element simulations, a double-lap bonded joint is considered to demonstrate the PD predictive capability for crack nucleation and

growth. Although a uniform temperature distribution is considered as part of the verification process, this study is also capable of including non-uniform temperature variations.

2. Peridynamic equation of motion

The generalized PD equation of motion is a nonlinear integro-differential equation in time and space in the form (Silling et al., 2007)

$$\rho(\mathbf{x})\ddot{\mathbf{u}}(\mathbf{x},t)=\int_{H_{\mathbf{x}}}\left(\mathbf{t}\left(\mathbf{u}'-\mathbf{u},\mathbf{x}'-\mathbf{x},t\right)-\mathbf{t}'\left(\mathbf{u}-\mathbf{u}',\mathbf{x}-\mathbf{x}',t\right)\right)dH_{\mathbf{x}}+\mathbf{b}(\mathbf{x},t), \tag{1}$$

where the region H defining the range of material point $\mathbf{x}$ is specified by δ, referred to as the "horizon." This equation can also be derived based on the principle of virtual work by satisfying the Lagrange's equation (Madenci and Oterkus, 2014). As shown by Silling and Lehoucq (2008), the classical theory of elasticity can be considered a limiting case of the PD theory as the horizon approaches zero in Eq. (1). Since the integrand in Eq. (1) does not contain any spatial derivatives, it is valid everywhere regardless of the presence of discontinuities. This equation is not usually amenable for analytical solutions. Therefore, its solution is constructed by using numerical techniques for spatial and time integrations. The spatial integration is performed by using the collocation method of a meshless scheme due to its simplicity. Hence, this equation is discretized by replacing the integration with an infinite summation as

$$\rho_{(k)}\ddot{\mathbf{u}}_{(k)}=\sum_{j=1}^{\infty}\left[\mathbf{t}_{(k)(j)}\left(\mathbf{u}_{(j)}-\mathbf{u}_{(k)},\mathbf{x}_{(j)}-\mathbf{x}_{(k)},t\right)-\mathbf{t}_{(j)(k)}\left(\mathbf{u}_{(k)}-\mathbf{u}_{(j)},\mathbf{x}_{(k)}-\mathbf{x}_{(j)},t\right)\right]V_{(j)}+\mathbf{b}_{(k)} \tag{2}$$

However, the numerical integration is performed by dividing the domain into a finite number of specific volumes associated with the integration (material) points, N. The volume of each point is assumed equal to each other. Therefore, this equation is rewritten to reflect the range of summation, N which has a fixed value representing the number of material points in the horizon of material point, $\mathbf{x}_{(k)}$ as

$$\rho_{(k)}\ddot{\mathbf{u}}_{(k)} = \sum_{j=1}^{N}\left[\mathbf{t}_{(k)(j)}\left(\mathbf{u}_{(j)} - \mathbf{u}_{(k)}, \mathbf{x}_{(j)} - \mathbf{x}_{(k)}, t\right) - \mathbf{t}_{(j)(k)}\left(\mathbf{u}_{(k)} - \mathbf{u}_{(j)}, \mathbf{x}_{(k)} - \mathbf{x}_{(j)}, t\right)\right]V_{(j)} + \mathbf{b}_{(k)} \tag{3}$$

where the displacement $\mathbf{u}_{(k)}$ is the displacement vector, and $\mathbf{b}_{(k)}$ is the body load vector at the material point $\mathbf{x}_{(k)}$. The vectors $\mathbf{t}_{(k)(j)}$ and $\mathbf{t}_{(j)(k)}$ represent the force density acting on material points $\mathbf{x}_{(k)}$ and $\mathbf{x}_{(j)}$, respectively. These force density vectors are unequal in magnitude with opposite directions. The family of material point $\mathbf{x}_{(k)}$ and $\mathbf{x}_{(j)}$ are denoted by $H_{\mathbf{x}_{(k)}}$ and $H_{\mathbf{x}_{(j)}}$, respectively, as shown in Fig.1 As illustrated in Fig. 2, the material point $\mathbf{x}_{(k)}$ interacts with its family of material points, $H_{\mathbf{x}_{(k)}}$, and it is influenced by the collective deformation of all these material points. Similarly, material point $\mathbf{x}_{(j)}$ is influenced by deformation of the material points, $H_{\mathbf{x}_{(j)}}$, in its own family. The number of family members in each family remains the same, and their motion conforms to the Lagrangian.

As proposed by Silling (2000), the horizon can be determined by matching the PD dispersion curves with those measured for a specific material. Weckner and Silling (2011) matched dispersion curves from the PD and atomistic simulations. However, such a horizon was on the order of the atomic spacing. Therefore, the PD horizon can be viewed as an *"effective interaction distance"* or an *"effective length-scale"* of a continuum model, and it may depend on the material properties, geometry and loading.

The horizon is related to the grid size. Therefore, Tian and Du (2014) developed Asymptotically Compatible (AC) discretization schemes for robust approximations of PD models and their local continuum models. AC schemes allow for the preservation of the consistency between nonlocal and local limits of the continuum model at the discrete level, regardless of how the grid spacing between the material points is compared with the horizon.

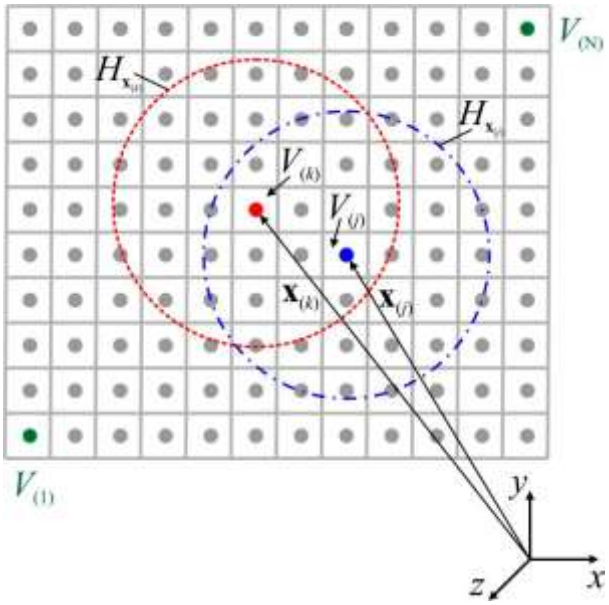

Figure 1. PD material points and interaction of points at $\mathbf{x}_{(k)}$ and $\mathbf{x}_{(j)}$.

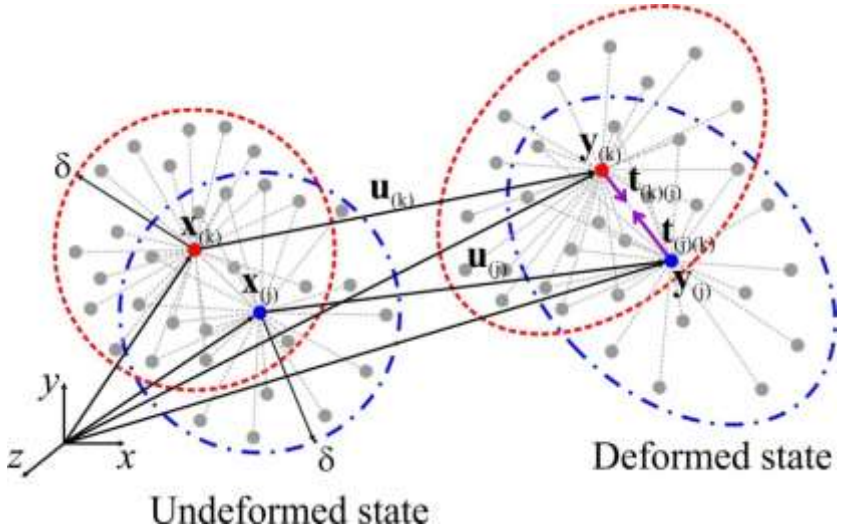

Figure 2. PD material points $\mathbf{x}_{(k)}$ and $\mathbf{x}_{(j)}$ influenced by the collective deformation of others in their families.

3. Peridynamic strain energy density

For an elastic and isotropic material, the PD Strain Energy Density (SED) in terms of deformation at a material point $\mathbf{x}_{(k)}$ can be expressed as (Madenci and Oterkus, 2016)

$$W_{(k)} = W_{(k)}^{\kappa} + W_{(k)}^{\mu}, \tag{4a}$$

where

$$W_{(k)}^{\kappa} = a_{\kappa}\theta_{(k)}^{2} \tag{4b}$$

and

$$W_{(k)}^{\mu} = \left\{ b\sum_{j=1}^{N} \Omega_{(k)(j)} \left(\left| \mathbf{y}_{(j)} - \mathbf{y}_{(k)} \right| - \left| \mathbf{x}_{(j)} - \mathbf{x}_{(k)} \right| \right)^{2} V_{(j)} - a_{\mu}\theta_{(k)}^{2} \right\}, \tag{4c}$$

with $W_{(k)}^{\kappa}$ and $W_{(k)}^{\mu}$ representing the dilatational and distortional parts of the strain energy density, and a_{κ}, a_{μ}, b, and d the material parameters. Under the assumption of small displacements and small rotations, the dilatation $\theta_{(k)}$ can be expressed in discrete form as

$$\theta_{(k)} = d\sum_{j=1}^{N} \Omega_{(k)(j)} \left(\left| \mathbf{y}_{(j)} - \mathbf{y}_{(k)} \right| - \left| \mathbf{x}_{(j)} - \mathbf{x}_{(k)} \right| \right) V_{(j)} \ , \tag{5}$$

Madenci and Oterkus (2014) gave, the influence function, $\Omega_{(k)(j)}$, in the form

$$\Omega_{(k)(j)} = \frac{\delta}{\left| \mathbf{x}_{(j)} - \mathbf{x}_{(k)} \right|} \ . \tag{6}$$

They also determined the PD parameters a_{κ}, a_{μ}, b, and d in terms of engineering material constants by considering two simple loading conditions: isotropic expansion and simple shear. Their specific expressions are derived by Madenci and Oterkus (2014) in the form

$$a_{\kappa} = \frac{1}{2}\kappa, \ a_{\mu} = \frac{5\mu}{6}, \ b = \frac{15\mu}{2\pi\delta^{5}}, \text{ and } d = \frac{9}{4\pi\delta^{4}} \quad \text{for (3-D)}, \tag{7a}$$

$$a_\kappa = \kappa\,,\ a_\mu = 2\mu\,,\ b = \frac{6\mu}{\pi h\delta^4}\,,\ \text{and}\ d = \frac{2}{\pi h\delta^3}\quad \text{for (2-D),} \tag{7b}$$

$$a_\kappa = 0\,,\ a_\mu = 0\,,\ b = \frac{E}{2\delta^3 A}\,,\ \text{and}\ d = \frac{1}{2\delta^2 A}\quad \text{for (1-D),} \tag{7c}$$

with κ and μ representing the bulk modulus and shear modulus of the material. The parameters h and A represent the thickness and cross-sectional area of the structure, respectively. The values of these parameters depend on the horizon size, and the dimension of the analysis. Although the SED given in Eq. (4) appears to be the same as that of the linear peridynamic solid suggested by Silling et al. (2007, it is different. The SED expression, Eq. (4) is strictly calibrated against the classical SED by considering a particular weight function given in Eq. (6), and it recovers the bond-based approach when dilatation is not distinguished. It is worth noting that the PD material parameters are determined for material points whose horizons are completely embedded in the material. In other words, they are only valid for a material point whose horizon is not truncated due to the presence of a boundary surface. Otherwise, they need to be corrected in order to account for the loss of family members within the horizon, as explained in Madenci and Oterkus (2016). The correction of the material parameters is achieved by numerically integrating both dilatation and strain energy density at each material point inside the body for simple loading conditions and comparing them to their counterparts obtained from classical continuum mechanics. There exist different methods for correcting the PD material parameters, and they are inherently all approximate. Recently, Mitchell et al. (2015) introduced the position-aware "*linear PD solid material model*" with a built-in surface correction procedure. It employs two different influence functions which are position-aware; they are different for material points near the surface and in the bulk. This study employs the correction procedure described by Madenci and Oterkus (2016).

4. Force density-stretch relations for thermoelastic deformation

As derived by Madenci and Oterkus (2014), the force density vector, $\mathbf{t}_{(k)(j)}$, at material point $\mathbf{x}_{(k)}$ can be obtained from

$$\mathbf{t}_{(k)(j)}\left(\mathbf{u}_{(j)}-\mathbf{u}_{(k)},\mathbf{x}_{(j)}-\mathbf{x}_{(k)},t\right)=\frac{1}{V_{(j)}}\frac{\partial W_{(k)}}{\partial\left(\left|\mathbf{y}_{(j)}-\mathbf{y}_{(k)}\right|\right)}\frac{\mathbf{y}_{(j)}-\mathbf{y}_{(k)}}{\left|\mathbf{y}_{(j)}-\mathbf{y}_{(k)}\right|}, \tag{8a}$$

which leads to the force density vector in the form

$$\mathbf{t}_{(k)(j)}=t_{(k)(j)}\frac{\mathbf{y}_{(j)}-\mathbf{y}_{(k)}}{\left|\mathbf{y}_{(j)}-\mathbf{y}_{(k)}\right|}, \tag{8b}$$

where

$$t_{(k)(j)}=2\delta d\frac{1}{\left|\mathbf{x}_{(j)}-\mathbf{x}_{(k)}\right|}\left(\left(a_{\kappa}-a_{\mu}\right)\theta_{(k)}-\frac{1}{2}a_2T_{(k)}\right)+2\delta b\left(s_{(k)(j)}-\alpha T_{(k)}\right). \tag{8c}$$

in which

$$a_2=a_{\alpha}(a_{\kappa}-a_{\mu}) \tag{8d}$$

with

$$a_{\alpha}=6\alpha \quad \text{for (3-D)} \tag{8e}$$

and

$$a_{\alpha}=4\alpha \quad \text{for (2-D)} \tag{8f}$$

The temperature change at material point $\mathbf{x}_{(k)}$ is $T_{(k)}$ with α representing the coefficient of thermal expansion. The stretch, $s_{(k)(j)}$, between material points $\mathbf{x}_{(k)}$ and $\mathbf{x}_{(j)}$ is defined as

$$s_{(k)(j)} = \frac{\left|\mathbf{y}_{(j)} - \mathbf{y}_{(k)}\right| - \left|\mathbf{x}_{(j)} - \mathbf{x}_{(k)}\right|}{\left|\mathbf{x}_{(j)} - \mathbf{x}_{(k)}\right|}. \tag{9}$$

The dilatation, $\theta_{(k)}$ at material point $\mathbf{x}_{(k)}$ can be defined as

$$\theta_{(k)} = d\delta \sum_{j=1}^{N} \left(s_{(k)(j)} - \alpha T_{(k)} \right) V_{(j)} + b_\alpha T_{(k)}. \tag{10a}$$

with

$$b_\alpha = 3\alpha \quad \text{for (3-D)} \tag{10b}$$

and

$$b_\alpha = 2\alpha \quad \text{for (2-D)} \tag{10c}$$

The force density vector can be decomposed into its dilatational and distortional parts as

$$\mathbf{t}_{(k)(j)} = \mathbf{t}^{\kappa}_{(k)(j)} + \mathbf{t}^{\mu}_{(k)(j)}, \tag{11a}$$

where

$$\mathbf{t}^{\kappa}_{(k)(j)} = \left(2\delta a_\kappa d \frac{1}{\left|\mathbf{x}_{(j)} - \mathbf{x}_{(k)}\right|} \theta_{(k)} - a_\alpha \delta a_\kappa d \frac{1}{\left|\mathbf{x}_{(j)} - \mathbf{x}_{(k)}\right|} T_{(k)} \right) \frac{\mathbf{y}_{(j)} - \mathbf{y}_{(k)}}{\left|\mathbf{y}_{(j)} - \mathbf{y}_{(k)}\right|} \tag{11b}$$

and

$$\mathbf{t}^{\mu}_{(k)(j)} = 2\delta b \left(\left(s_{(k)(j)} - \alpha T_{(k)} \right) - a_\mu \frac{d}{b} \left(\theta_{(k)} - \frac{a_\alpha}{2} T_{(k)} \right) \frac{1}{\left|\mathbf{x}_{(j)} - \mathbf{x}_{(k)}\right|} \right) \frac{\mathbf{y}_{(j)} - \mathbf{y}_{(k)}}{\left|\mathbf{y}_{(j)} - \mathbf{y}_{(k)}\right|}. \tag{11c}$$

Similarly, the total stretch can also be decomposed into its dilatational and distortional parts as (Madenci and Oterkus, 2016)

$$s_{(k)(j)} = s^{\kappa}_{(k)(j)} + s^{\mu}_{(k)(j)}, \tag{12}$$

The distortional stretch, $s^{\mu}_{(k)(j)}$, can be expressed as

$$s^{\mu}_{(k)(j)} = \left(s_{(k)(j)} - \alpha T_{(k)}\right) - a_{\mu}\frac{d}{b}\left(\theta_{(k)} - \frac{a_{\alpha}}{2}T_{(k)}\right)\frac{1}{\left|\mathbf{x}_{(j)} - \mathbf{x}_{(k)}\right|}. \tag{13}$$

$$s^{\mu}_{(k)(j)} = s_{(k)(j)} - s^{\kappa}_{(k)(j)}. \tag{13}$$

Finally, substituting from Eq. (13) into Eq. (11) permits the force density vector in terms of its dilatational and distortional parts as

$$\mathbf{t}_{(k)(j)} = \left(\frac{2\delta a_{\kappa} d}{\left|\mathbf{x}_{(j)} - \mathbf{x}_{(k)}\right|}\theta_{(k)} - \frac{a_{\alpha}\delta a_{\kappa} d}{\left|\mathbf{x}_{(j)} - \mathbf{x}_{(k)}\right|}T_{(k)} + 2\delta b s^{\mu}_{(k)(j)}\right)\frac{\mathbf{y}_{(j)} - \mathbf{y}_{(k)}}{\left|\mathbf{y}_{(j)} - \mathbf{y}_{(k)}\right|}, \tag{14}$$

5. Peridynamic force density for thermoviscoelastic deformation

The correspondence principle is used to establish the force density for a linear viscoelastic isotropic material based on the isotropic linear elastic materials. If a body experiences a viscoelastic deformation, the force density, Eq. (14) can be expressed in terms of Boltzmann hereditary superposition integral as

$$t_{(k)(j)} = \frac{2\delta d}{\left|\mathbf{x}_{(j)} - \mathbf{x}_{(k)}\right|}\int_0^t a_{\kappa}\left(t - t'\right)\frac{\partial \theta_{(k)}}{\partial t'}dt' - \frac{a_{\alpha}\delta d}{\left|\mathbf{x}_{(j)} - \mathbf{x}_{(k)}\right|}\int_0^t a_{\kappa}\left(t - t'\right)\frac{\partial T_{(k)}}{\partial t'}dt' + 2\delta\int_0^t b\left(t - t'\right)\frac{\partial s^{\mu}_{(k)(j)}}{\partial t'}dt' \tag{15a}$$

In accordance with Eq. (7), the peridynamic parameters, $a_\kappa(t)$, $a_\mu(t)$ and $b(t)$ depend on either the bulk modulus, $\kappa(t)$ or shear modulus, $\mu(t)$. They can be expressed in the form of Prony series as

$$\kappa(t) = \kappa_\infty + \sum_{i=1}^{N} \kappa_i e^{-t/\tau_i} \tag{15b}$$

and

$$\mu(t) = \mu_\infty + \sum_{i=1}^{N} \mu_i e^{-t/\tau_i} \tag{15b}$$

The first terms in these expressions represent their asymptotic values, and the parameter, τ_i represents the relaxation time.

For thermorheologically simple materials, the change in temperature can be transformed to the change in time scale by shifting the relaxation time with a shift function, Φ (Haddad, 1995). One of the widely used shift function is the WLF (Williams-Landel-Ferry) shift function (Williams, 1955) given as

$$\log \Phi = -\frac{c_1 \left(T - T_o\right)}{c_2 + \left(T - T_o\right)} \tag{16a}$$

where c_1 and c_2 are material constants, T_0 is usually the glass transition temperature. Therefore, the relaxation time is scaled as

$$\tau_i = \frac{\tau_i^0}{\Phi} \tag{16b}$$

where τ_i^0 is the relaxation time at $T = T_0$.

If the bulk modulus, κ is assumed to be independent of time, the dilatational and distortional parts of the force density become

$$t^{\kappa}_{(k)(j)} = \left(\frac{2\delta a_{\kappa} d}{\left|\mathbf{x}_{(j)} - \mathbf{x}_{(k)}\right|} \theta_{(k)} - \frac{a_{\alpha}\delta a_{\kappa} d}{\left|\mathbf{x}_{(j)} - \mathbf{x}_{(k)}\right|} T_{(k)} \right) \tag{17}$$

and

$$t^{\mu}_{(k)(j)} = \int_0^t 2\delta b_{\infty} \frac{\partial s^{\mu}_{(k)(j)}}{\partial t'} dt' + \sum_{i=1}^{N} b_i \int_0^t 2\delta e^{-(t-t')/\tau_i} \frac{\partial s^{\mu}_{(k)(j)}}{\partial t'} dt' \tag{18}$$

After adding and subtracting $\sum_{i=1}^{N} 2\delta b_i \int_0^t \frac{\partial s^{\mu}_{(k)(j)}}{\partial t'} dt'$ to Eq. (18), performing algebraic manipulations leads to

$$t^{\mu}_{(k)(j)} = \int_0^t 2\delta \left[b_{\infty} + \sum_{i=1}^{N} b_i \right] \frac{\partial s^{\mu}_{(k)(j)}}{\partial t'} dt' - \sum_{i=1}^{N} 2\delta b_i \int_0^t \left[1 - e^{-(t-t')/\tau_i} \right] \frac{\partial s^{\mu}_{(k)(j)}}{\partial t'} dt' \tag{19}$$

Defining $\gamma_i^{(k)(j)}$ as the viscous stretch, this equation can be rewritten as

$$t^{\mu}_{(k)(j)} = 2\delta b_0 s^{\mu}_{(k)(j)} - \sum_{i=1}^{N} 2\delta b_i \gamma_i^{(k)(j)}(t) \tag{20a}$$

in which

$$\gamma_i^{(k)(j)}(t) = \int_0^t \left[1 - e^{-(t-t')/\tau_i} \right] \frac{\partial s^{\mu}_{(k)(j)}}{\partial t'} dt' \tag{20b}$$

and

$$b_0 = b_\infty + \sum_{i=1}^{N} b_i \tag{20c}$$

The superscripts of $\gamma_i^{(k)(j)}$ represents the interaction between material points $\mathbf{x}_{(k)}$ and $\mathbf{x}_{(j)}$, and the subscript i represents the terms in the Prony series.

In order to perform the numerical time integration, the viscous stretch is discretized as explained in the ABAQUS 6.12 Theory Manual (Section 4.8.1).

$$\gamma_i^{(k)(j)}(t_{n+1}) = \int_0^{t_n} \left[1 - e^{-(t_{n+1}-t')/\tau_i}\right] \frac{\partial s^{\mu}_{(k)(j)}}{\partial t'} dt' + \int_{t_n}^{t_{n+1}} \left[1 - e^{-(t_{n+1}-t')/\tau_i}\right] \frac{\partial s^{\mu}_{(k)(j)}}{\partial t'} dt' \tag{21a}$$

in which the second term can be approximated as

$$\int_{t_n}^{t_{n+1}} \left[1 - e^{-(t_{n+1}-t')/\tau_i}\right] \frac{\partial s^{\mu}_{(k)(j)}}{\partial t'} dt' = \Delta s^{\mu}_{(k)(j)} - \tau_i \left[1 - e^{-\Delta t/\tau_i}\right] \frac{\Delta s^{\mu}_{(k)(j)}}{\Delta t} \tag{21b}$$

under the assumption that $s^{\mu}_{(k)(j)}$ varies linearly with time, i.e.,

$$\frac{ds^{\mu}_{(k)(j)}}{dt'} = \frac{\Delta s^{\mu}_{(k)(j)}}{\Delta t'} \tag{21c}$$

Also, the first term on the right side of Eq. (21a) can be evaluated as

$$\int_0^{t_n} \left[1 - e^{-(t_{n+1}-t')/\tau_i}\right] \frac{\partial s^{\mu}_{(k)(j)}}{\partial t'} dt' = \left[1 - e^{-\Delta t/\tau_i}\right] s^{\mu}_{(k)(j)} + e^{-\Delta t/\tau_i} \gamma_i^{(k)(j)}(t_n) \tag{22}$$

Subsequently, the viscous stretch can be expressed as

$$\gamma_i^{(k)(j)}(t_{n+1}) = \left[1-e^{-\Delta t/\tau_i}\right] s^{\mu}_{(k)(j)} + \Delta s^{\mu}_{(k)(j)} + e^{-\Delta t/\tau_i}\gamma_i^{(k)(j)}(t_n) - \tau_i\left[1-e^{-\Delta t/\tau_i}\right]\frac{\Delta s^{\mu}_{(k)(j)}}{\Delta t} \tag{23}$$

With the following approximation

$$e^{-\Delta t/\tau_i} = 1-\left(\frac{\Delta t}{\tau_i}\right)+\frac{1}{2}\left(\frac{\Delta t}{\tau_i}\right)^2, \tag{24a}$$

as $\Delta t/\tau_i \to 0$, the viscous stretch can be finally rewritten as

$$\gamma_i^{(k)(j)}(t_{n+1}) = \gamma_i^{(k)(j)}\left(t_n\right)+\left(\frac{\Delta t}{\tau_i}\right)\left(s^{\mu}_{(k)(j)} - \gamma_i^{(k)(j)}(t_n)\right)+\frac{\Delta s^{\mu}_{(k)(j)}}{2}\left(\frac{\Delta t}{\tau_i}\right) \tag{24b}$$

6. Failure criteria

A failure process is included in the analysis by monitoring the interaction between two material points, $\mathbf{x}$ and $\mathbf{x}'$ as suggested by Silling and Askari (2005). Their interaction can be terminated based on a particular criteria; thus, leading to the removal of their PD force from the equations of motion by introducing the function $\mu\left(\mathbf{x}'-\mathbf{x},t\right)$ as

$$\rho(\mathbf{x})\ddot{\mathbf{u}}(\mathbf{x},t) = \int_H \psi\left(\mathbf{x}'-\mathbf{x},t\right)\left(\mathbf{t}\left(\mathbf{u}'-\mathbf{u},\mathbf{x}'-\mathbf{x},t\right)-\mathbf{t}'\left(\mathbf{u}-\mathbf{u}',\mathbf{x}-\mathbf{x}',t\right)\right)dH_{\mathbf{x}'}+\mathbf{b}\left(\mathbf{x},t\right) \tag{25a}$$

where

$$\psi\left(\mathbf{x}'-\mathbf{x},t\right) = \begin{cases} 1 & \text{if interaction exists,} \\ 0 & \text{if no interaction.} \end{cases} \tag{25b}$$

In the case of viscoelastic deformation, the force density between two material points, $\mathbf{x}_{(k)}$ and $\mathbf{x}_{(j)}$, exhibits a time dependent behavior. Thus, the corresponding work done by the interaction between these points, referred to as "viscoelastic micropotential", $w_{(k)(j)}$ can be expressed as

$$w_{(k)(j)}(t) = w_{0^+(k)(j)} + w_{v(k)(j)}(t) \tag{26}$$

in which $w_{0^+(k)(j)}$ and $w_{v(k)(j)}$ represent the instantaneous elastic and viscous components of the micropotential. The viscoelastic micropotential can be determined as

$$w_{(k)(j)}(t) = \int_0^{s_{(k)(j)}(t=0^+)} t_{0^+(k)(j)} \left|\mathbf{x}_j - \mathbf{x}_k\right| ds_{(k)(j)} + \int_{s_{(k)(j)}(t=0^+)}^{s_{(k)(j)}(t)} t_{(k)(j)}(t) \left|\mathbf{x}_j - \mathbf{x}_k\right| ds_{(k)(j)} \tag{27}$$

in which $t_{0^+(k)(j)}$ represents the instantaneous elastic force density.

In order to create a new crack surface, A_c, all of the micropotentials between the material points $\mathbf{x}_{(k^+)}$ and $\mathbf{x}_{(j^-)}$ whose line of action crosses this new surface must be terminated (Fig. 3). The material points $\mathbf{x}_{(k^+)}$ and $\mathbf{x}_{(j^-)}$ are located above and below the new crack surface, respectively. The number of material points within the family of $\mathbf{x}_{(k^+)}$ below the crack surface and intersecting with the crack is denoted by K^-. Similarly, J^+ represents the number of material points above the crack surface within the family of $\mathbf{x}_{(j^-)}$ and intersecting with the crack. In this figure, the green and red points represent the material points $\mathbf{x}_{(k^+)}$ and $\mathbf{x}_{(j^-)}$ located above and below the potential crack surface, respectively.

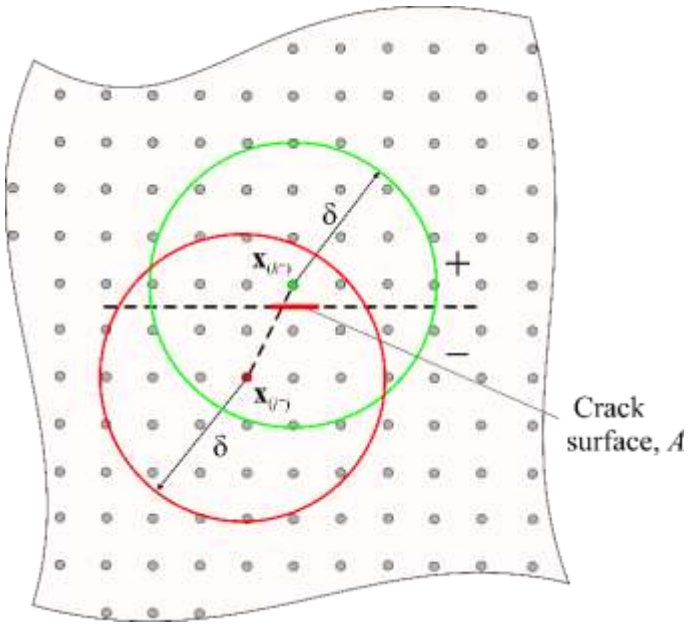

Figure 3. Interaction across a crack surface between material points $\mathbf{x}_{(k^+)}$ and $\mathbf{x}_{(j^-)}$.

The strain energy required to remove the interaction between the two material points, $\mathbf{x}_{(k^+)}$ and $\mathbf{x}_{(j^-)}$, can be expressed as

$$W_{(k^+)} = \frac{1}{2}\frac{w_{(k^+)(j^-)} + w_{(j^-)(k^+)}}{2} V_{(k^+)} V_{(j^-)}. \tag{28}$$

The micropotential due to this interaction is assumed as their average value, and the corresponding strain energy density is split equally. Furthermore, the total strain energy required to remove all of the interactions across the crack surface A_c can be obtained as

$$W(t) = \frac{1}{2}\sum_{k=1}^{K^+}\frac{1}{2}\sum_{j=1}^{J^-} w_{(k^+)(j^-)} V_{(k^+)} V_{(j^-)} + \frac{1}{2}\sum_{k=1}^{K^+}\frac{1}{2}\sum_{j=1}^{J^-} w_{(j^-)(k^+)} V_{(j^-)} V_{(k^+)}, \tag{29}$$

for which the line of interaction defined by $|\mathbf{x}_{(k^+)} - \mathbf{x}_{(j^-)}|$ and the crack surface intersect, and K^+ indicates the number of material points above and J^- the number below the crack surface within

the families of $\mathbf{x}_{(k^+)}$ and $\mathbf{x}_{(j^-)}$, respectively. If this line of interaction and crack surface intersect at the crack tip, only half of the critical micropotential is considered in the summation. The expression in Eq. (29) can be simplified as

$$W(t) = \frac{1}{2}\sum_{k=1}^{K^+}\sum_{j=1}^{J^-}\frac{1}{2}\left(w_{(k^+)(j^-)} + w_{(j^-)(k^+)}\right)V_{(k^+)}V_{(j^-)} \tag{30}$$

Substituting for micropotentials given by Eq. (27) in Eq. (30) results in the strain energy required to eliminate all of the interactions across the unit crack surface, $A_c = h\Delta x$, with Δx representing the spacing between the material points and h the thickness.

The total work, $W(t)$, required to eliminate all interactions across this new surface can be related to the energy release rate as

$$G(t) = \frac{1}{2}\sum_{k=1}^{K^+}\sum_{j=1}^{J^-}\frac{1}{2}\left(G_{(k^+)(j^-)} + G_{(j^-)(k^+)}\right) \tag{31a}$$

where

$$\begin{aligned} G_{(k^+)(j^-)} &= \frac{1}{(\Delta x)h} w_{(k^+)(j^-)} V_{(k^+)} V_{(j^-)} \\ G_{(j^-)(k^+)} &= \frac{1}{(\Delta x)h} w_{(j^-)(k^+)} V_{(k^+)} V_{(j^-)} \end{aligned} \tag{31b}$$

For a horizon size of $\delta = 3\Delta x$, the number of material points above and below the crack surfaces is $K^+ = J^- = 9$. As shown in Fig. 8, a point indicated with a red circle below the crack has 22 interactions with points indicated with green and yellow circles above the crack surface. All of these interactions cross the crack surfaces. However, 10 such interactions with the yellow points pass through the crack tip, and only half of their strain energy is used for creating a new crack surface. Therefore, the number of full interactions contributing to the generation of a unit crack

surface of $A_c = \Delta x$ becomes 17. Similarly, there exist 17 full interactions for a point located above the crack surface. Thus, the total number of interactions, N_c creating a unit crack surface becomes 34.

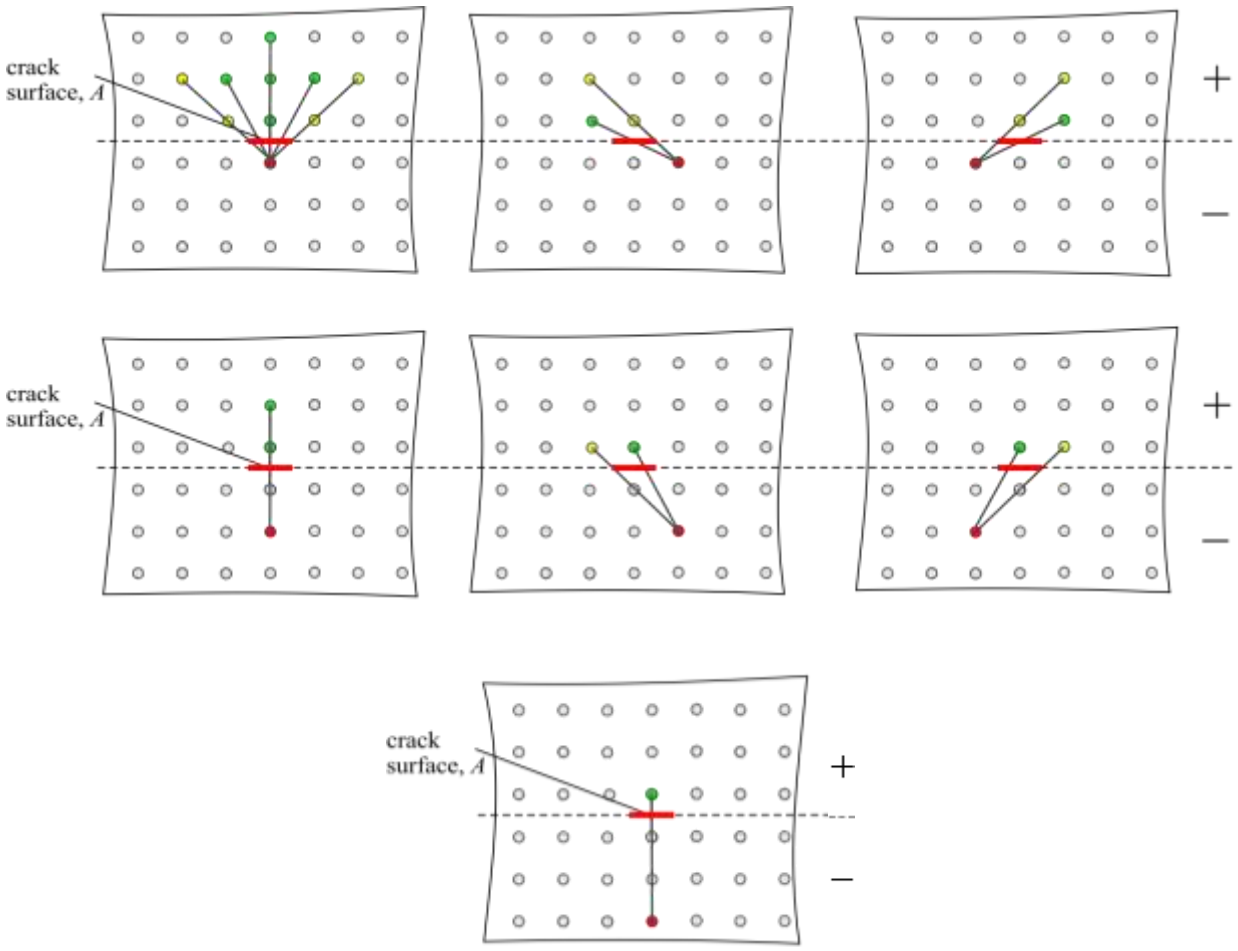

Figure 4. Interactions of material points above the crack surface interacting with the material points below the crack surface.

The measured critical value, G_c, of the material defines the amount of energy required to remove all interactions, leading to

$$G_c = \frac{1}{2}\sum_{k=1}^{K^+}\sum_{j=1}^{J^-}\frac{1}{2}\left(G^c_{(k^+)(j^-)} + G^c_{(j^-)(k^+)}\right) \tag{32}$$

Peridynamics enables the simulation of damage propagation by progressively removing the interactions between materials points. In order to reflect this feature, the critical energy release rate, G_c, of a material point is distributed equally to each interaction at that material point (Hu et al., 2015). Note that the explicit determination of the critical stretch, s_c, is not required in the numerical implementation of the PD analysis. Under the assumption of $G^c_{(k^+)(j^-)} \approx G^c_{(j^-)(k^+)}$, the failure criteria for each interaction can be expressed as

$$G_{(k)(j)} \geq G^c_{(k)(j)} \tag{33a}$$

with

$$G^c_{(k^+)(j^-)} = \frac{G_c}{N_c} \tag{33b}$$

This approach is not specific to viscoelastic deformation. It can be used for elastic and elastic-plastic deformation as demonstrated by Hu et al. (2015) and Madenci and Oterkus (2016). For the rate-dependent materials such as polymers, the critical energy release rate is rate-dependent and usually it increases with the increase of loading rate. For example, Guojun (2007) measured the critical energy release rate for an epoxy molding compound commonly used in integrated circuit (IC) packages as

$$G_c = G_0(1+10\dot{\varepsilon}-1.3\dot{\varepsilon}) \tag{34}$$

where $G_0 = 5.2$ N/m at a loading rate of $\dot{\varepsilon} = 0$. It is worth mentioning that the present study does not include the rate effect.

Local damage, which defines the ratio of eliminated interactions to the total number of interactions associated with a material point within its horizon, can be calculated as (Silling and Askari, 2005)

$$\varphi\left(\mathbf{x}_{(i)},t\right)=1-\frac{\sum_{j=1}^{N}\psi\left(\mathbf{x}_{(j)}-\mathbf{x}_{(i)},t\right)V_{(j)}}{\sum_{j=1}^{N}V_{(j)}} \tag{35}$$

Local damage has a value between 0 and 1. No damage at that material point is denoted by $\varphi=0$, while $\varphi=1$ denotes that all the interactions are eliminated with the related material point. Moreover, $\varphi=0.5$ denotes that half of the interactions are eliminated with the related material point.

7. Numerical procedure

The solution to the PD equation of motion requires spatial integration, which is performed by using a Gaussian integration (meshless) scheme. The domain is divided into a uniform grid, with material (integration or collocation) points associated with specific volumes. The solution of PD equation of motion is obtained through Euler explicit time integration. However, the effect of inertial forces in the equation of motion is disregarded while considering the time dependent behavior of the material. Therefore, the quasi-static solution is achieved by using the adaptive dynamic relaxation (ADR) method described by Kilic and Madenci (2010) for each time increment. The damping term used in the ADR method has a fictitious value to ensure that the solution converges to the static solution in a short amount of time. This damping term is not related to the viscoelastic terms. The solution algorithm concerns the calculation of the viscoelastic terms within each time step of the ADR method. It is achieved by performing the following steps:

(1) Calculate viscous stretch by using Eq. (24a)
(2) Calculate total stretch by using Eq. (9)
(3) Calculate distortional stretch by using Eq. (13)
(4) Calculate dilatational stretch
(5) Calculate dilatational part of the force density
(6) Calculate distortional part of the force density by using Eq. (20a)

The convergence of PD solutions depends on the horizon size and spacing between the material points as described by Bobaru et al. (2009). The horizon size is specified as $\delta = m\Delta x$ with Δx representing the uniform spacing between the collocation points.

8. Numerical results

Numerical results first concern a viscoelastic plate under either uniform tension or simple shear loading. It is then subjected to a combined simple shear and uniform temperature change. Next, crack nucleation and growth prediction capability is demonstrated by considering a double-lap joint with a viscoelastic adhesive and elastic adherent materials under tension. In all of the numericals results, the viscoelastic material is made of epoxy. Its bulk response, $\kappa(t)$ is assumed elastic $\kappa(t) = \kappa$, and the shear response, $\mu(t)$ is viscoelastic as specified in Eq. (42). As measured by Guojun (2007), the coefficients of the Prony series for the Young's modulus of epoxy are specified in Table 1. These values are used to compute the shear modulus for a Poisson's ratio, $\nu = 0.3$. It has a mass density of $\rho = 1810\,\text{kg/m}^3$. Its thermal expansion coefficient is specified as $\alpha = 50\times10^{-6}\,1/\,^oC$. Also, the parameters in shift function in Eq. (16a) are chosen as (Guojun, 2007)

$$c_1 = 30,\ c_2 = 100,\ T_o = 110^oC \tag{44}$$

Its mode II critical strain energy release rate is specified as $G_c = 5.2\,\text{N/m}$ (Guojun, 2007).

The displacement and traction boundary conditions are imposed through a nonzero volume of fictitious boundary layers as described by Madenci and Oterkus (2016). The spatial integration is performed by adopting the procedure described by Madenci and Oterkus (2014) for a circular domain of interaction (family size) with a horizon size of $\delta = m\Delta x$.

During the iterations, the ADR time step is specified as one. However, the time integration related to the material response is achieved with a real time step of $\Delta t = 1\times10^{-4}\,\text{s}$. In order to verify the PD predictions, these problems are also analyzed by using ANSYS, a commercially available finite

element analysis software. The finite element predictions are achieved by employing element type Plane 182, and with a time step size of $1\times10^{-4}s$.

Table 1. Prony series coefficients for the relaxation modulus of epoxy (Guojun, 2007).

i	τ_i	E_i (Mpa)
1	1.00E-04	200
2	1.00E-03	800
3	1.00E-02	1500
4	1.00E+00	1000
5	1.00E+01	1100
6	1.00E+02	2700
7	1.00E+03	2900
8	1.00E+04	2500
9	1.00E+05	900
10	1.00E+06	950
11	1.00E+07	600
12	1.00E+08	120
13	1.00E+09	180
14	1.00E+11	200
15	3.00E+12	250
	E_∞	700

8. 1 Rectangular plate under either tension or simple shear

The length and width of the plate are specified as $L=0.3\text{m}$ and $W=0.15\text{m}$, respectively, with thickness, $h=0.003\text{m}$. The origin of the Cartesian coordinate system coincides with the lower left corner of the plate as shown in Figure 5. In the case of uniform tension, the plate is constrained by roller-type supports along the left end. It is suddenly subjected to uniform tensile stress along the right end, and the load is released after 0.005 s. These boundary conditions are enforced as

$$u(x=0,y,t)=0 \tag{45a}$$

$$\sigma_{xx}(x=L,y,t)=\sigma_o H(t-0.005) \tag{45b}$$

In the case of uniform shear loading, the plate is subjected to uniform shear loading along the right and left edges. These boundary conditions are enforced as

$$u(x=0,y,t)=0 \tag{46a}$$

$$u(x=L,y,t)=0 \tag{46b}$$

$$\sigma_{xy}(x=0,y,t)=-\sigma_o H(t-0.005) \tag{46c}$$

$$\sigma_{xy}(x=L,y,t)=\sigma_o H(t-0.005) \tag{46d}$$

where $\sigma_o = 2000\,\text{Pa}$.

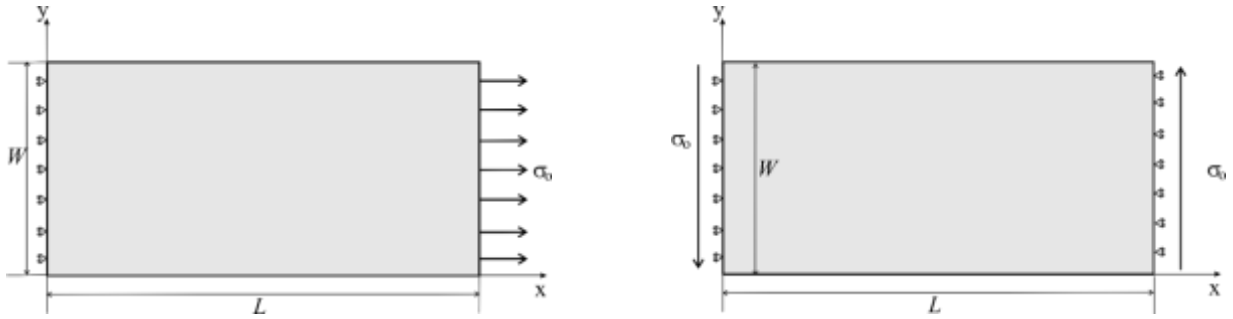

(a) (b)

Figure 5. Plate geometry and loading: (a) tension, and (b) shear

The spacing, Δx between the material points and the parameter m defining horizon size are determined based a convergence study. Fig. 6 shows the convergence of the solutions for a fixed horizon size $\delta = 0.015\,\text{m}$ with varying $m = 1,2,3$. The PD predictions converge to the ANSYS solution for $m = 3$. Based on this value of $m = 3$, Fig. 7 shows the convergence of the PD predictions for varying spacing of $\Delta x = 0.015, 0.0075, 0.005, 0.003\,\text{m}$. Therefore, the PD

computational model is generated with a uniform grid of 100×50 material (integration) points with a value of $m=3$. For both loading conditions, the PD predictions capture the instaneous elastic response at $t=0^{+}$ as well as the creep and recovery responses as shown in Fig. 8 and 9. They compare well with the predictions by ANSYS.

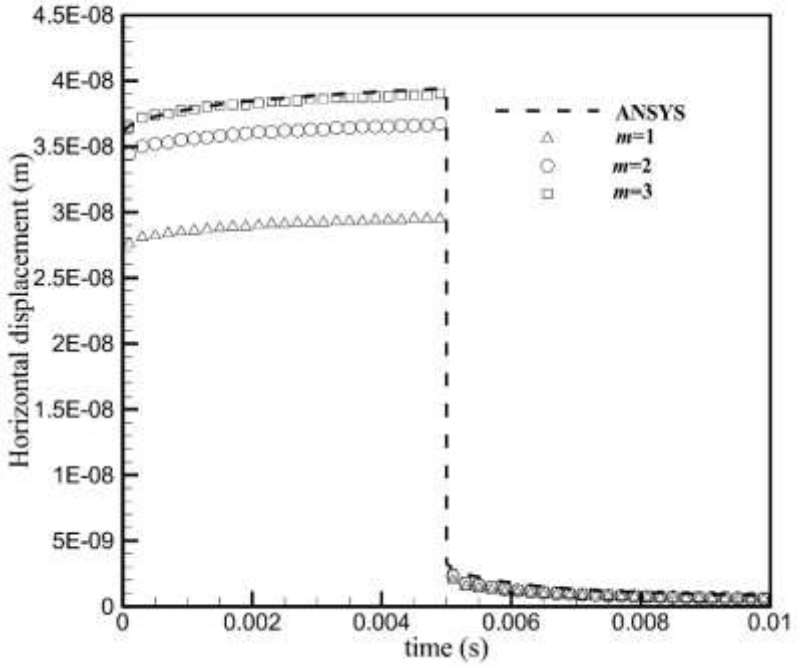

Figure 6. Convergence of PD predictions with a fixed value of horizon $\delta=0.015$ for varying $m=1,2,3$

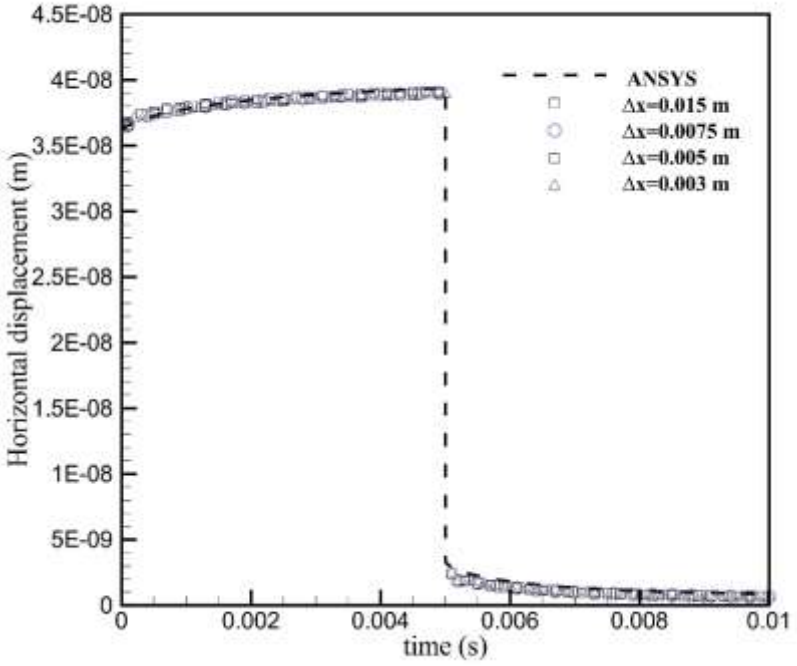

Figure 7. Convergence of PD predictions with a fixed value of $m = 3$ for varying Δx.

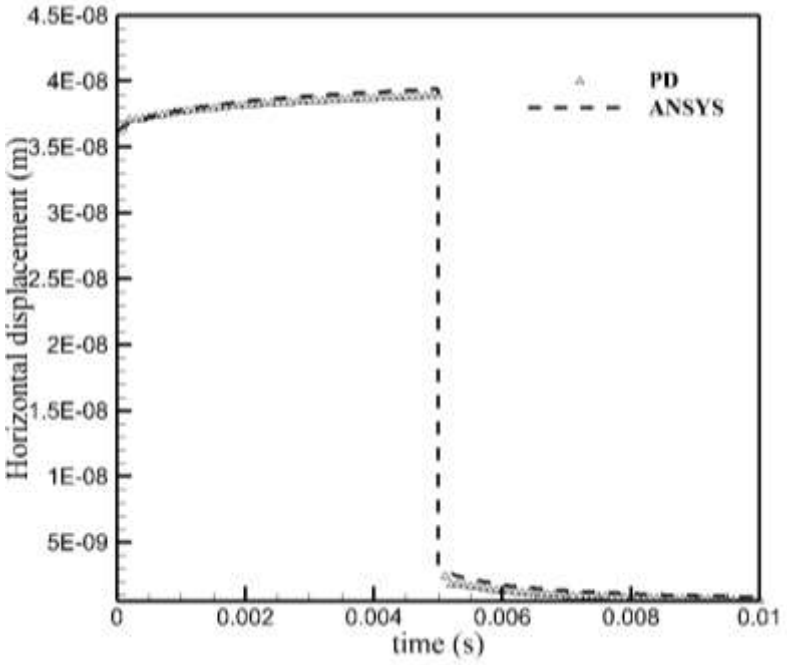

Figure 8. Horizontal displacement versus time at $(x, y) = (L, W/2)$ for a plate under tension

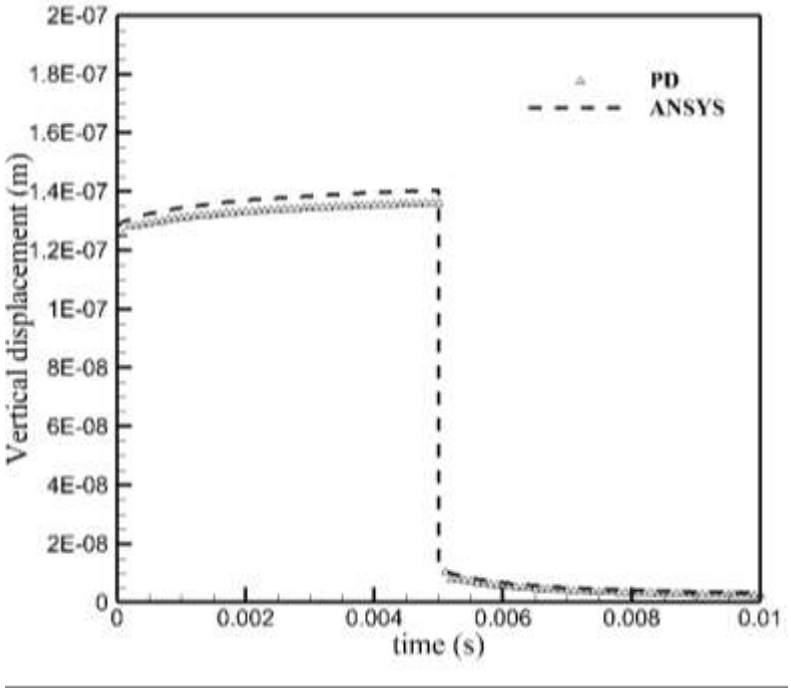

Figure 9. Vertical displacement versus time at $(x, y) = (L, W/2)$ for a plate under shear:

8. 2 Rectangular plate under simple shear and constant temperature

The plate is subjected to uniform temperature of $T = 200^{\circ}\mathrm{C}$, and simple shear loading is achieved by the conditions given by Eq. (46) with $\sigma_o = 1\mathrm{MPa}$. For such a combined loading, the PD predictions accurately capture the horizontal and vertical displacements as shown in Fig. 10. These predictions compare extremely well with the FEA predictions.

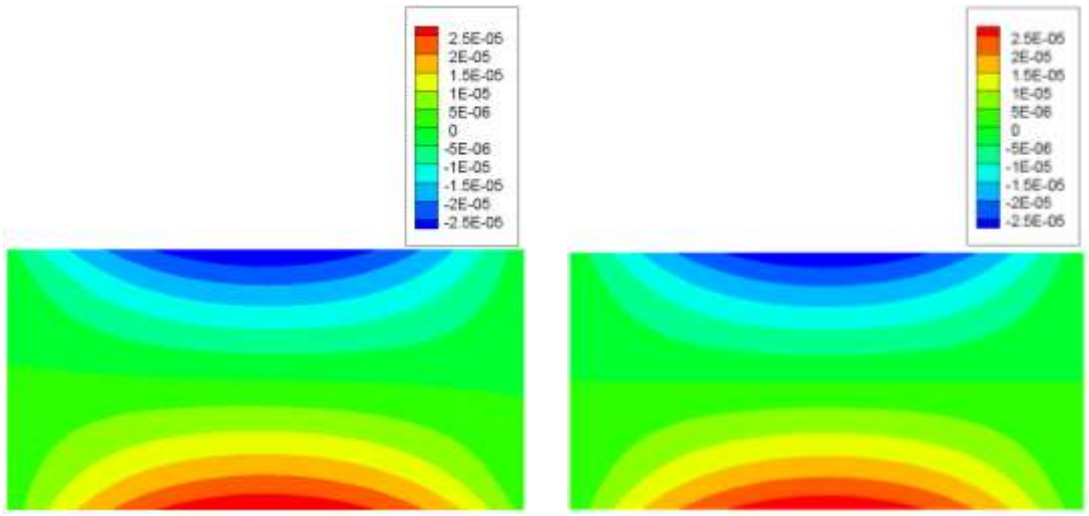

(a) (b)

Figure 10. Horizontal displacement field at $t = 10 \times 10^{-4}\,\mathrm{s}$: (a) PD and (b) ANSYS

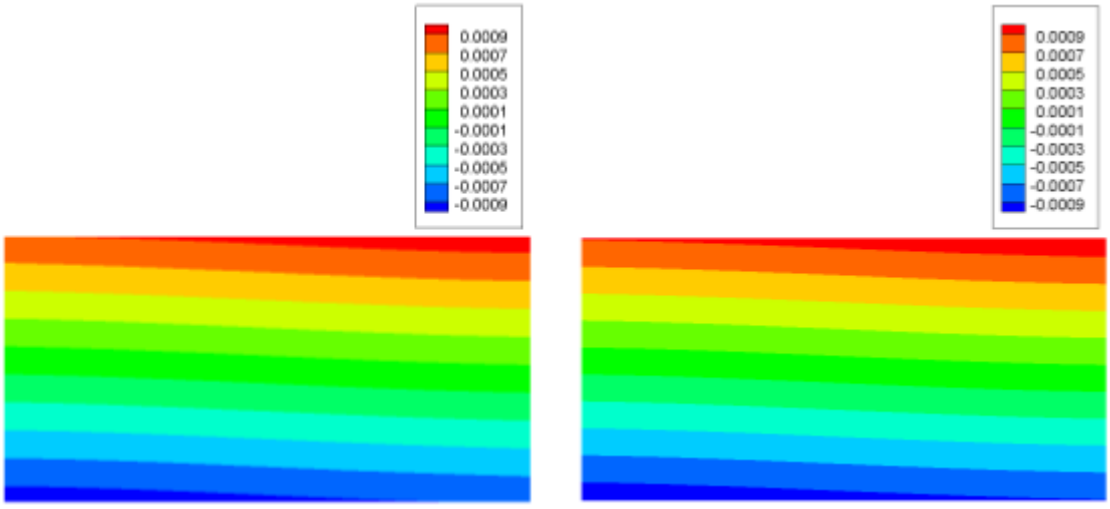

(a) (b)

Figure 11. Vertical displacement field at $t = 10 \times 10^{-4}\,\mathrm{s}$: (a) PD and (b) ANSYS

8. 3 Double-lap joint under tension

The double-lap bonded joint geometry is described in Fig. 12. The dimensions are specified as $a = b = 2c = 2t = 4h = 8\,\mathrm{mm}$. The adhesive is viscoelastic and adherents are elastic with Young's modulus, $E = 70\,\mathrm{GPa}$ and Poisson's ratio, $\nu = 0.3$. The lap joint is subjected to uniform tension

at the right and left edges with $\sigma_{xx} = \sigma_o = 7\,\text{MPa}$. The force density vector arising due to the interaction of two material points across the interface between the adhesive and adherent is calculated through their average. Due to the presence of symmetry, only one quarter of the geometry is modeled. The load is kept constant during the simulation. As shown in Fig. 13, the crack nucleates and grows along the bond line immediately after the application of the load at the lower corner of the adhesive joint. These predictions are based on the constant value of the critical energy release rate for epoxy as given in Eq. (34). For decreasing horizon, the PD prediction consistently leads to failure initiation at the location high stress concentration.

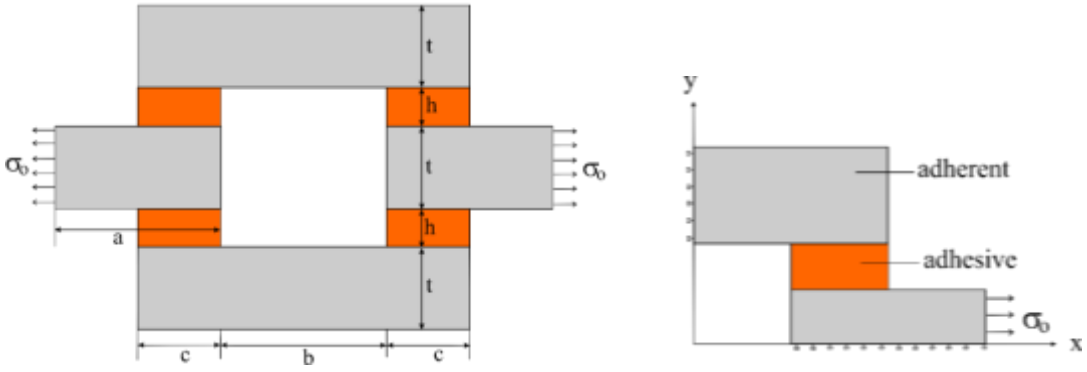

Figure 12. Bonded double-lap joint geometry and PD model due to symmetry

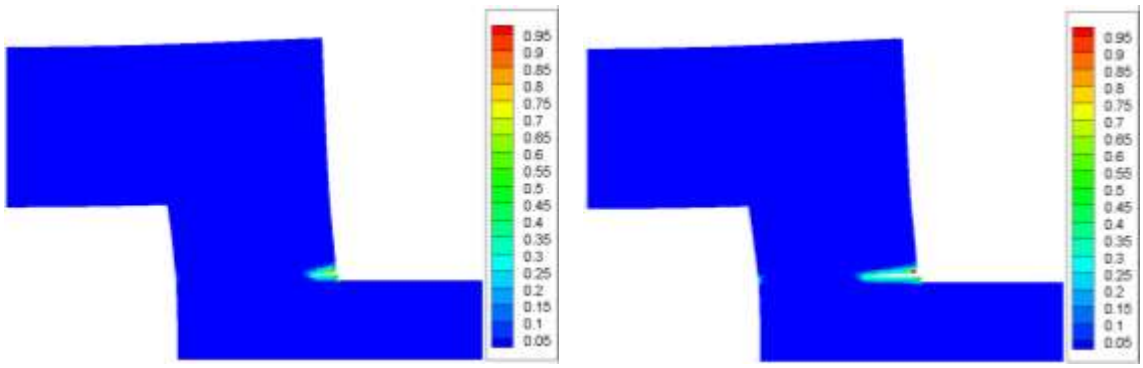

(a) (b)

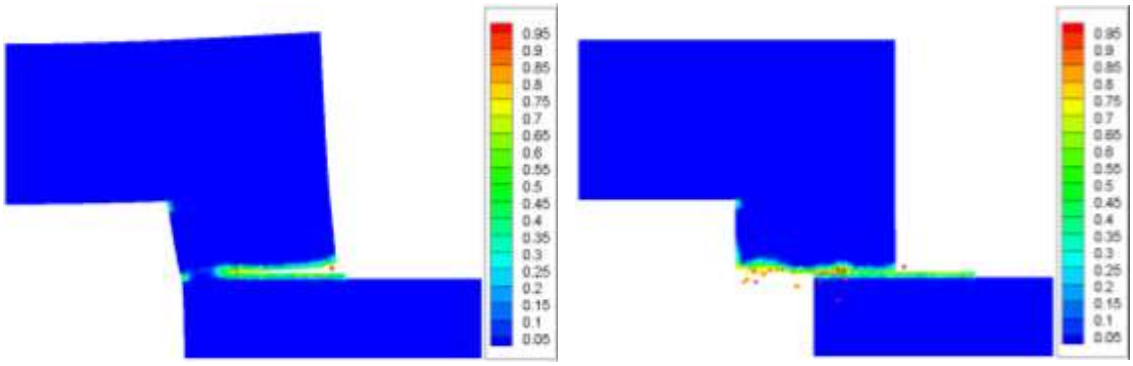

(c) (d)

Figure 13. Damage prediction at a) $t = 10 \times 10^{-4} s$, b) $t = 20 \times 10^{-4} s$, c) $t = 30 \times 10^{-4} s$, and d) $t = 40 \times 10^{-4} s$ (Displacements are magnified by 100 for the deformed configurations)

9. Concluding Remarks

This study presents an ordinary state-based PD model of viscoelastic materials in terms of Prony series. The constitutive constants are the same as those needed in the classical history-integral model. Also, it presents a failure criteria based on the viscoelastic micropotential of each interaction. The critical stretch critical energy release rate for each interaction is implicitly determined, and can vary depending on the degree of viscoelastic deformation. The critical value to remove the interaction is related to the critical value of the energy release rate of the material. The validity of PD predictions is established by considering benchmark solutions concerning a

plate under either tension or shear, and combined shear and thermal loading as well as a double-lap joint under tension. The PD viscoelastic deformation analysis successfully captures the relaxation behavior of the material.

Acknowledgments

This study was performed as part of the ongoing research at the MURI Center for Material Failure Prediction through Peridynamics at the University of Arizona (AFOSR Grant No. FA9550-14-1-0073; Program Managers: Drs. David Stargel, A. Sayir, and F. Fahroo).

References

ABAQUS 6.12 Theory Manual-https://things.maths.cam.ac.uk/computing/software/abaqus_docs/docs/v6.12

Bobaru, F., Yang, M., Alves, L. F., Silling, S. A., Askari, E., Xu, J. (2009) Convergence, adaptive refinement, and scaling in 1D peridynamics, *Int. J. for Numer. Meth. in Eng*. Vol. 77, pp 852-877.

Guojun, H. (2007) A theoretical and Numerical study of crack propagation along a bimaterial interface with application to IC packaging, National University of Singapore, (PhD dissertation).

Haddad, Y. M. (1995) Viscoelasticity of engineering materials, *Chapman & Hall*, New York.

Hu, Y. L., De Carvalho, N. V., and Madenci, E. (2015) Peridynamic modeling of delamination growth in composite laminates, *Composite Structures*, *132*, 610-620.

Kilic, B., Madenci, E., (2010) An adaptive dynamic relaxation method for quasi-static simulations using the peridynamic theory, *Theor. Appl. Fract. Mech*. Vol. 53, pp. 194-201.

Madenci, E., Oterkus, E., (2014) Peridynamic Theory and Its Applications, *Springer,* New York.

Madenci, E., and Oterkus, S. (2016) Ordinary state-based peridynamics for plastic deformation according to von Mises yield criteria with isotropic hardening, *J. Mech. Phys. Solids*, Vol. 86, pp. 192-219.

Mitchell, J.A. (2011) A non-local, ordinary-state-based viscoelasticity model for peridynamics, *SAND2011-8064*, Sandia National Laboratories, Albuquerque.

Mitchell, J.A., Silling, S.A. and Littlewood, D.J. (2015) A Position-Aware Linear Solid Constitutive Model for Peridynamics, *J. of Mechanics of Materials and Structures*, Vol. 10, pp. 539-557

Silling, S.A. (2000) Reformulation of elasticity theory for discontinuities and long-range forces, *J. Mech. Phys. Solids*, Vol. 48, pp. 175-209.

Silling, S.A. and Askari, E. (2005) A meshfree method based on the peridynamic model of solid mechanics, *Comput. Struct.* Vol. 83, pp. 526-1535.

Silling, S.A., Epton, M., Weckner, O., Xu, J., and Askari, A. (2007) Peridynamics states and constitutive modeling, *J. Elast.* Vol. 88, pp. 151–184.

Silling, S.A. and Lehoucq, R.B. (2008) Convergence of peridynamics to classical elasticity theory, *J. Elast*. Vol. 93, pp. 13-37.

Tian, X. and Du, Q. (2014) Asymptotically compatible schemes and applications to robust discretization of nonlocal models, *SIAM J. Numer. Anal*., Vol. 52, pp.1641-1665.

Weckner, O., and Mohamed, N. A. N. (2013) Viscoelastic material models in peridynamics, *App. Math. and Comp.*, Vol. 219, pp. 6039-6043.

Weckner, O., Silling, S.A. (2011). Determination of nonlocal constitutive equations from phonon dispersion relations. *Int. J. Multiscale Com. Eng.*, Vol. 9**,** pp. 623-634.

Williams, M.L., Landel R. F., and Ferry J. D. (1955) The temperature dependence of relaxation mechanisms in amorphous polymers and and other glass-forming liquids, *J. of the Amer. Chem. Soc*., Vol. 77, pp. 3701-3707.